

# Formation of Foam-like Microstructural Carbon by Carbonization of Porous Coordination Polymers via Ligand-assisted Foaming Process

Kanokwan Kongpatpanich,<sup>[a]</sup> Satoshi Horike,<sup>\*,[a]</sup> Yu-ichi Fujiwara,<sup>[a],[b]</sup> Naoki Ogiwara,<sup>[a]</sup> Hirotomo Nishihara,<sup>[c]</sup> Susumu Kitagawa<sup>\*,[a],[d]</sup>

<sup>[a]</sup> Department of Synthetic Chemistry and Biological Chemistry, Graduate School of Engineering, Kyoto University, Kyoto, 615-8510, Japan

<sup>[b]</sup> Functional Materials Science Research Laboratories, Research & Development Headquarters, Lion Co. Ltd., Tokyo, 132-0035, Japan

<sup>[c]</sup> Institute of Multidisciplinary Research for Advanced Materials, Tohoku University, Sendai, 980-8577, Japan

<sup>[d]</sup> Institute for Integrated Cell-Material Science (WPI-iCeMS), Kyoto University, Kyoto, 615-8501, Japan

**Abstract:** Porous carbon with a foam-like microstructure has been synthesized by direct carbonization of porous coordination polymer (PCP). In situ generation of foaming agents by chemical reactions of ligands in PCP during carbonization provides a simple way to create lightweight carbon with a foam-like microstructure. Among several substituents, the nitro group has been proved to be the key to obtain the unique foam-like microstructure due to the fast kinetics of gas evolution during carbonization. Foam-like microstructural carbons showed higher specific capacitance compared to a microporous carbon.

polymer foams.<sup>[7]</sup> However, laser ablation requires complicated instrumentation, and only a limited number of polymer foams can produce carbon foam through carbonization. Alternatively, our approach to prepare a foam-like microstructure of porous carbon is through the reaction of organic ligands in PCP/MOFs during carbonization. Gas evolution from organic ligands could then act as gas pockets, directing foam-like microstructures. As porous carbon has been widely used as an electrode for electrochemical double layer capacitance (EDLC), we demonstrated that a foam-like microstructure could improve the EDLC performance of porous carbon.

## Introduction

Porous carbon is attracting attention due to its potential applications in many fields ranging from gas storage, electrochemical catalysts and supercapacitors.<sup>[1]</sup> Carbonization of carbon precursors accommodated in inorganic templates is a common method used to prepare porous carbon.<sup>[2]</sup> Among many templates available, crystalline porous coordination polymer (PCP) or metal-organic framework (MOF) has gained particular attention in recent years because of its organic-inorganic alternating structure.<sup>[3]</sup> Although there are many reports on the preparation of carbon with high surface area or good electrochemical properties from PCP/MOFs,<sup>[4]</sup> there is still a lack of fundamental understanding on the effect of organic ligands in PCP/MOFs controlling pore structure and morphology of the resulting carbon. It is challenging to prepare carbons with a variety of morphologies, microstructures and porous properties in a predictable manner by selecting suitable combinations of metal ions and organic ligands in PCP/MOFs. One interesting microstructure is carbon foam, which is a sponge-like carbon material attractive for many aerospace and industrial applications as it is lightweight.<sup>[5]</sup> Carbon foam is prepared by either laser ablation of carbon substrates<sup>[6]</sup> or carbonization of

## Results and Discussion

We used PCPs with an interdigitated motif of 2D layers because of their ability to incorporate a variety of 5-substituted isophthalate (*R*-ip) ligands without altering the overall framework topology.<sup>[8]</sup> Three compounds with different substituents, [Zn(5-*R*-isophthalate)(4,4'-bipyridyl)]<sub>n</sub> (CID-*R*, where *R* = H, OCH<sub>3</sub>, NO<sub>2</sub>), were synthesized according to previously reported procedures.<sup>[8a, 9]</sup> We chose isophthalate derivatives containing methoxy and nitro groups because they undergo exothermic decomposition, and show gas evolution upon heating beyond their decomposition temperatures.<sup>[10]</sup> All guest-free CID-*R* have similar packing structures and block-type crystal morphologies as shown in **Figure 1**. Oxygen atoms from four carboxylates coordinate to two Zn<sup>2+</sup> ions, with the axial position of each coordinated by the nitrogen atoms of 4,4'-bipyridyl (bpy), creating the 2D layered structure. The compounds are thermally stable up to 300 °C according to thermogravimetric (TG) analysis, and show weight loss between 300 and 500 °C (**Figure S1**). The first weight loss at 300 °C–380 °C is due to the release of bpy confirmed by the simultaneous measurement of TG and mass spectrometry (TG-MS). The second weight loss at

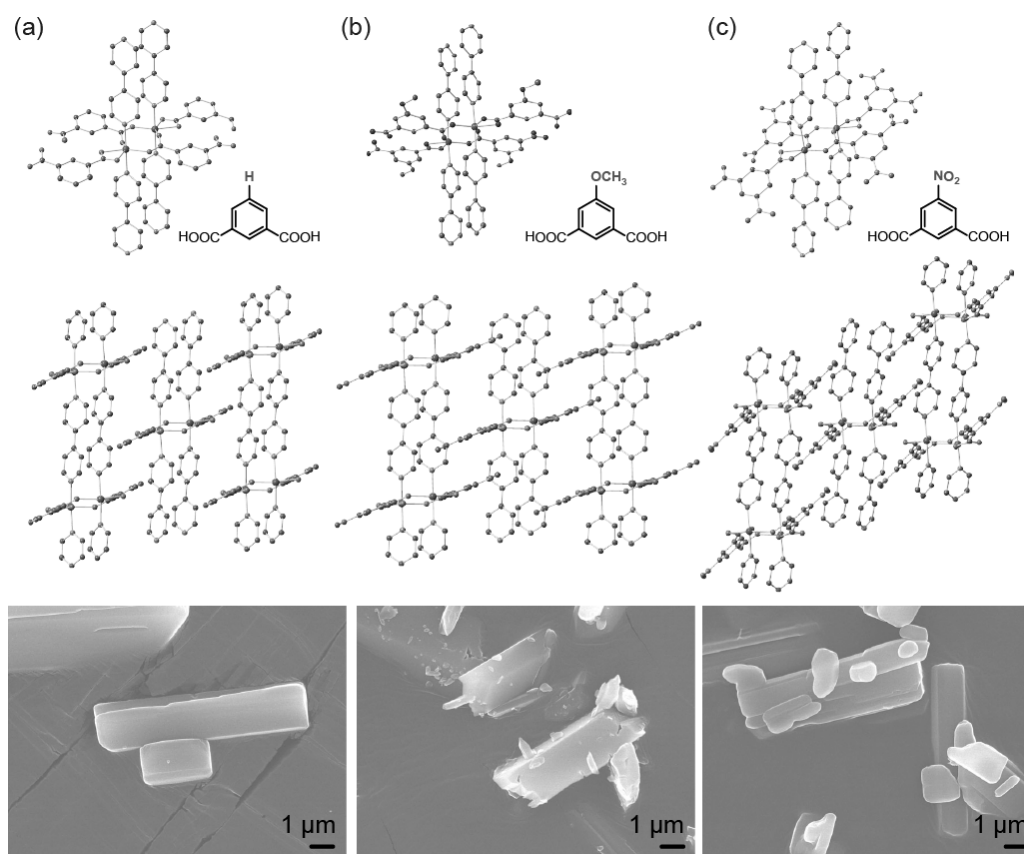


**Figure 1.** (From top) Coordination environment, packing structures, and scanning electron microscopy (SEM) images of the guest-free (a) CID-H, (b) CID-OCH<sub>3</sub>, and (c) CID-NO<sub>2</sub>.

temperature range of 400 °C–460 °C is caused by the decomposition of *R*-ip, which differs in each CID-*R* due to the different substituents. For CID-NO<sub>2</sub>, the second weight loss is accompanied by a sharp exothermic peak at 436 °C, which is due to the reaction of nitro group under thermal stimulus.

Zn-based PCPs are attractive choices for carbonization as ZnO in the resulting carbon can be removed without an acid washing process. ZnO is reduced to Zn metal during carbonization, and vaporized from the system beyond its boiling point. Carbonization of Zn-based PCPs is generally conducted at 1000 °C for several hours under an inert atmosphere as higher porosity tends to develop over the longer carbonization time.<sup>[11]</sup> We performed carbonization of three CID-*R* compounds at 1000 °C for 2 h; however, the product yields were either in very low or non-existent because of the vaporization of both inorganic and organic species. To obtain porous carbon, we employed a short carbonization time (15 min) at 800 °C and 1000 °C. We denote all carbonized samples as CID-*R*-*x*, where *R* indicates the substituent of *R*-ip and *x* represents the carbonization temperature. A total of six porous carbon were synthesized. CID-*R*-1000 samples are metal-free carbons and CID-*R*-800 samples are ZnO/carbon composites, as checked by powder X-ray diffraction (PXRD). The local structures of CID-*R*-1000 were studied by PXRD and Raman spectroscopy (**Figure S2** and **S3**).

All samples contained low crystalline carbon according to a broad diffraction peak ( $2\theta = 25^\circ$ ) belonging to an (002) interlayer of graphitic carbon.<sup>[3a]</sup> Raman spectra of all CID-*R*-1000 exhibit two bands with similar intensities assigned to the D and G bands, suggesting the presence of both disordered carbon and graphene sheet in the samples.<sup>[12]</sup>

We observed the microstructures of CID-*R*-*x* by transmission electron microscopy (TEM) (**Figure 2**). Comparison of TEM images of CID-*R*-800 and CID-*R*-1000 provided the understanding of how ZnO particles contribute to the different microstructures. Note that upon heating to 1000 °C, ZnO in CID-*R*-800 were reduced by carbon and completely vaporized resulting in the metal-free carbons (CID-*R*-1000). The pore structure in CID-OCH<sub>3</sub>-1000 clearly arises from the vaporization of ZnO, leaving empty space throughout the carbon domain. TEM images of CID-NO<sub>2</sub>-*x* in Figure 2e and 2f show a unique microstructure compared to those of CID-H-*x* and CID-OCH<sub>3</sub>-*x*. Both CID-NO<sub>2</sub>-800 and CID-NO<sub>2</sub>-1000 have a foam-like structure consisting of many macropores. The microstructure of CID-NO<sub>2</sub>-*x* is consistent with the lightweight character observed in the bulk phase (**Figure S4**). However, formation of ZnO is not related to the foam-like microstructure of CID-NO<sub>2</sub>-1000 as the microstructure is completely developed prior to the removal of ZnO by heat treatment.

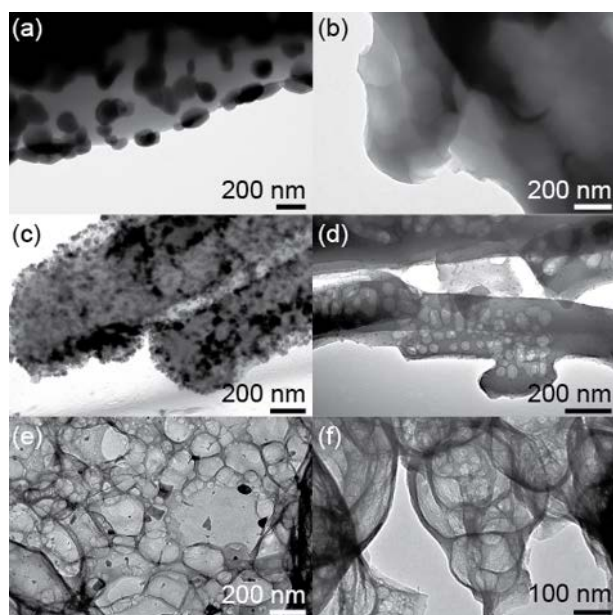


**Figure 2.** TEM images of (a) CID-H-800, (b) CID-H-1000, (c) CID-OCH<sub>3</sub>-800, (d) CID-OCH<sub>3</sub>-1000, (e) CID-NO<sub>2</sub>-800, and (f) CID-NO<sub>2</sub>-1000.

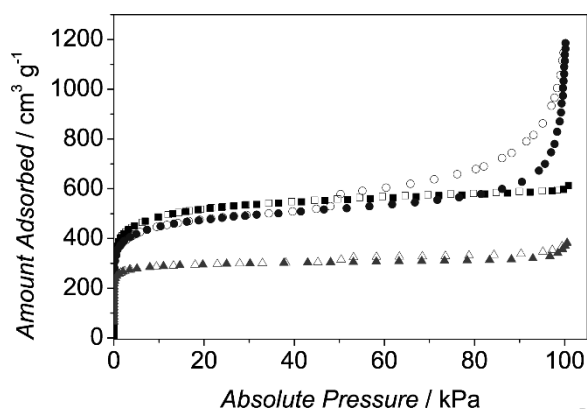


**Figure 3.** N<sub>2</sub> adsorption isotherms at 77 K for CID-H-1000 (squares), CID-OCH<sub>3</sub>-1000 (triangles), and CID-NO<sub>2</sub>-1000 (circles). Closed symbols are adsorption data and open symbols are desorption data.

We compared N<sub>2</sub> adsorption isotherms of CID-R-1000 samples to investigate the different porous properties resulting from different ligand substituents (**Figure 3**). The Brunauer, Emmett, and Teller (BET) surface area is in the range of 1100–1900 m<sup>2</sup> g<sup>-1</sup> (see **Table S1** for details). CID-R are non-porous, however, the resulting carbon have porous architectures. All adsorption isotherms are type I isotherms, which are typical for microporous materials.<sup>[13]</sup> CID-H-1000 is essentially microporous, whereas CID-OCH<sub>3</sub>-1000 is a microporous material with a hysteresis observed at higher pressure (**Figure S5**). CID-NO<sub>2</sub>-1000 contains high mesoporosity according to the mesopore distribution analysis (Barret-Joyner-Helenda (BJH) plot). Hysteresis between adsorption and desorption isotherms at higher pressure observed in CID-NO<sub>2</sub>-1000 also indicates

mesoporosity. The sharp N<sub>2</sub> uptake observed in CID-NO<sub>2</sub>-1000 at the pressure range of 90–100 kPa is due to a capillary condensation of N<sub>2</sub> in mesopores. Methoxy groups impair the porosity of the resulting carbon, in terms of the total pore volume and the degree of mesoporosity. Although the surface area of CID-NO<sub>2</sub>-1000 is slightly lower than CID-H-1000 (1746 vs 1902 m<sup>2</sup> g<sup>-1</sup>), the total pore volume of CID-NO<sub>2</sub>-1000 is double that of CID-H-1000. The significant increase in pore volume is undoubtedly contributes to the mesoporosity.

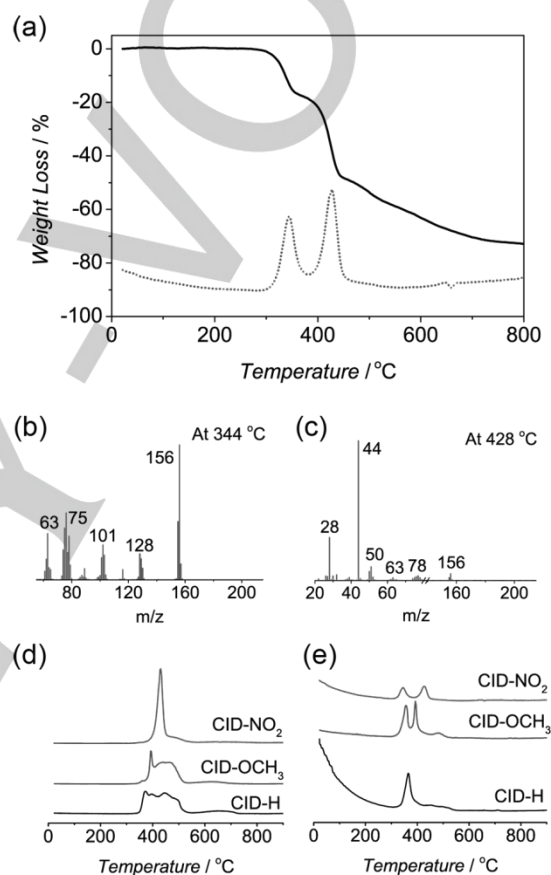


**Figure 4.** (a) TG-MS plot of CID-NO<sub>2</sub>. Mass spectra at (b) 344 °C and (c) at 428 °C. Ion chromatograms of (d)  $m/z = 44$  (CO<sub>2</sub>) and (e)  $m/z = 28$  (CO or N<sub>2</sub>).

The unique foam-like structure found in CID-NO<sub>2</sub>-1000 is attributed to the chemical process of nitro group during carbonization. We attempted to understand the stepwise processes in the carbonization of CID-R in order to clarify the origin of the foam-like microstructure and the differences in porosity. TG-MS analysis revealed the different chemical processes of CID-R occurred during carbonization (**Figure 4**). The first weight loss at 300 °C–380 °C in TG of all CID-R corresponds to bpy ( $m/z$  of 156) (**Figure S6**). Decomposition of R-ip occurred in the second weight loss (380 °C–460 °C) with major evolution of N<sub>2</sub>, CO and CO<sub>2</sub>. The minor species evolved in this temperature region are bpy and benzene, thus the

majority of benzene fragments in *R*-ip still remain to form porous carbon. Relatively broad peak was observed in the

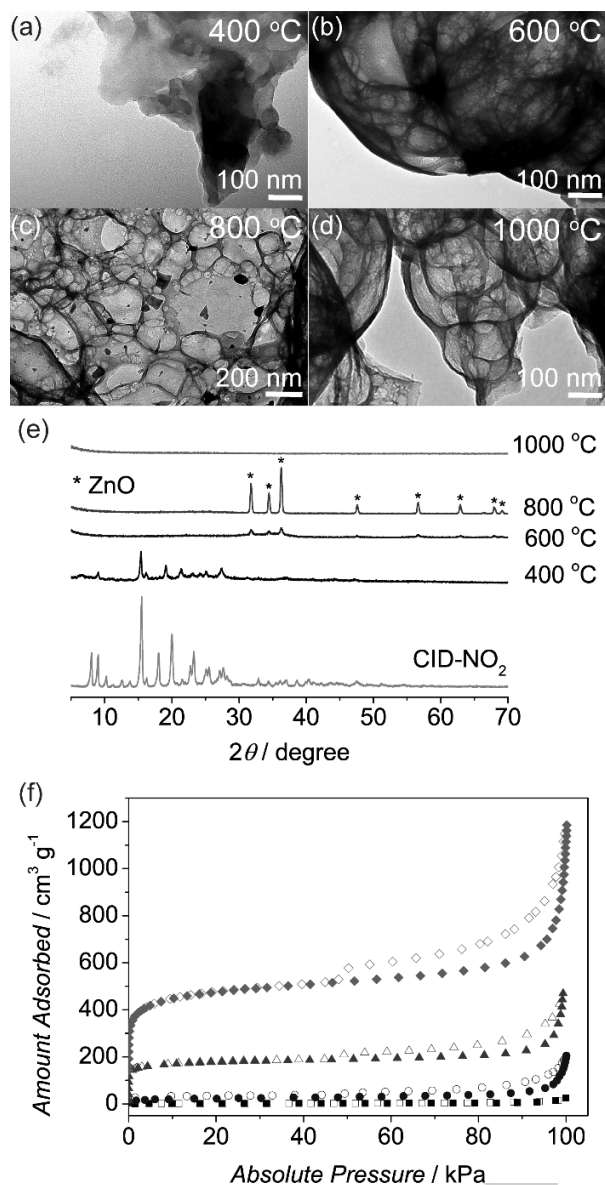


**Figure 5.** (a–d) TEM images of CID-NO<sub>2</sub>-400, CID-NO<sub>2</sub>-600, CID-NO<sub>2</sub>-800, and CID-NO<sub>2</sub>-1000. (e) PXRD patterns of CID-NO<sub>2</sub> carbonized at 400 °C–1000 °C. (f) N<sub>2</sub> adsorption isotherms at 77 K for CID-NO<sub>2</sub>-400 (squares), CID-NO<sub>2</sub>-600 (circles), CID-NO<sub>2</sub>-800 (triangles), and CID-NO<sub>2</sub>-1000 (diamonds).

mass spectrum ( $m/z$  of 44) of CID-OCH<sub>3</sub> at 380 °C–540 °C suggesting the slow kinetics of CO<sub>2</sub> evolution (Figure 4d). We assumed that the slow kinetics of CO<sub>2</sub> evolution decrease the porosity of CID-OCH<sub>3</sub>-1000. On the other hand, sharp peak was observed in case of CID-NO<sub>2</sub> at 400 °C–450 °C suggesting the faster kinetics of CO<sub>2</sub> evolution. The different kinetics of CO<sub>2</sub> evolution in CID-OCH<sub>3</sub> and CID-NO<sub>2</sub> is mainly due to the inductive effect of the substituents on the strength of carboxylate

groups in *R*-ip. Nitro group is a strong electron withdrawing group, decreases the electron density in benzene ring, and subsequently facilitates the breaking of C–C bond of the ring and carboxylate group. Methoxy group is an electron donating group, and has the opposite trend of CO<sub>2</sub> evolution. Additional N<sub>2</sub> evolution was observed in CID-NO<sub>2</sub> at 400 °C–450 °C supposing to be one of products from the reaction of nitro group (Figure 4e). We prepared four carbon samples from CID-NO<sub>2</sub> carbonized at 400 °C, 600 °C, 800 °C and 1000 °C (carbonization time of 15 min for all) to investigate the formation of the foam-like microstructure and the porous network (Figure 5). The foam-like microstructure was developed over the temperature range of 400 °C–600 °C, corresponding to the temperature range that NO<sub>2</sub>-ip moieties decompose with fast kinetics of CO<sub>2</sub> evolution. The mechanism to form this unique morphology is similar to polymer foaming process,<sup>[14]</sup> where the evolved CO<sub>2</sub> gases act as gas pockets in the inorganic/organic residues under kinetically favored conditions. The foam-like microstructure is retained at higher temperature as observed by TEM. Formation of ZnO and the porous carbon network occurred at 600 °C–1000 °C, according to PXRD and N<sub>2</sub> adsorption experiments. Mesopores tend to form consecutively during the decomposition of CID-NO<sub>2</sub> (ca. 400 °C–600 °C), followed by the formation of micropores at higher temperature regions (see Table S2 for details). ZnO was involved as the template to generate microporosity, as micropores mainly developed after ZnO was generated in the system.

We also tried carbonization of 5-nitroisophthalic acid (NO<sub>2</sub>-ip) under the same conditions, and could not obtain any products.

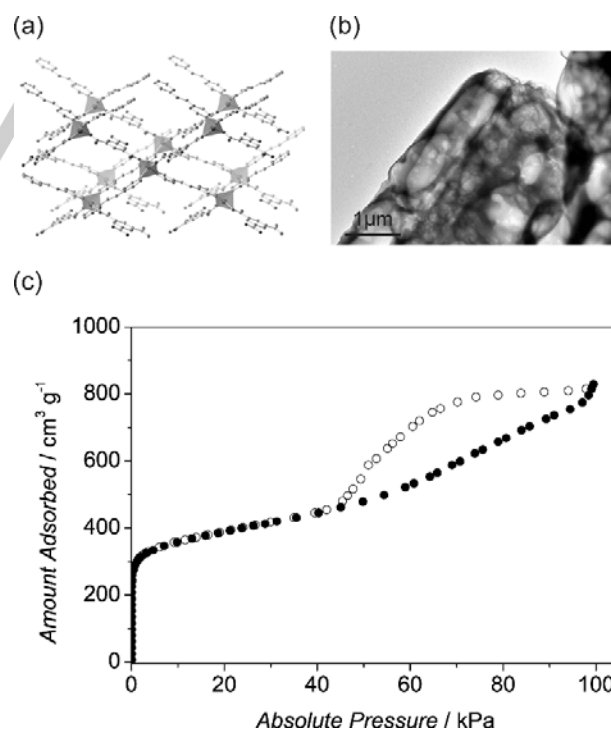


**Figure 6.** (a) Packing structure of [Zn(NO<sub>2</sub>-ip)(dpe)]<sub>n</sub>. (b) TEM image of [Zn(NO<sub>2</sub>-ip)(dpe)]<sub>n</sub> carbonized at 1000 °C. (c) N<sub>2</sub> adsorption isotherm at 77 K for [Zn(NO<sub>2</sub>-ip)(dpe)]<sub>n</sub> carbonized at 1000 °C

Thus, the incorporation of NO<sub>2</sub>-ip in PCP frameworks is essential to obtain porous carbon. We further confirmed the effect of the reaction from nitro-substituted ligand in PCPs to create porous carbon with a foam-like microstructure by use of another compound. [Zn(NO<sub>2</sub>-ip)(dpe)]<sub>n</sub> is constructed from Zn<sup>2+</sup>, NO<sub>2</sub>-ip, and 1,2-di(4-pyridyl)ethylene (dpe) (Figure 6).<sup>[15]</sup> The coordination environment around Zn<sup>2+</sup> and crystal topology of [Zn(NO<sub>2</sub>-ip)(dpe)]<sub>n</sub> are different from CID-NO<sub>2</sub>. The crystal structure of [Zn(NO<sub>2</sub>-ip)(dpe)]<sub>n</sub> consists of tetrahedral Zn<sup>2+</sup> coordinated to oxygen atoms of two NO<sub>2</sub>-ip moieties, and nitrogen atoms of two dpe ligands. The packing structure is the 3D reticular network with large void spaces, and each network is interpenetrated in a three-fold fashion. During the carbonization process, we observed N<sub>2</sub> and CO<sub>2</sub> evolution at 460 °C by TG-MS analysis (Figure S7), and carbon prepared from this compound (ZnNipdpe-1000) had a similar foam-like structure (Figure 6b). The obtained carbon had a BET surface area of 1946 m<sup>2</sup> g<sup>-1</sup> and a total pore volume of 1.71 cm<sup>3</sup> g<sup>-1</sup>, which is comparable to CID-NO<sub>2</sub>-1000. These results support the role of nitro-substituted organic ligands on the formation of a foam-like microstructure in porous carbon. Interestingly, ZnNipdpe-1000 has more uniform mesopores with a narrow pore size distribution (Figure S8). Although it is possible to control the microstructure of porous carbon including macropore characteristics by using appropriate reactions of organic ligands during carbonization, the crystal topology of PCP is another key factor for the control of nanopore characteristics of the resulting carbon.

We evaluated the impact of foam-like microstructure on the electrochemical performance of porous carbon by cyclic voltammetry (Figure 7). Cyclic voltammograms of CID-H-1000, CID-NO<sub>2</sub>-1000 and ZnNipdpe-1000 have rectangular shape, which is a characteristic pattern of EDLC. CID-NO<sub>2</sub>-1000 has higher specific capacitance than CID-H-1000. The enhancement of capacitance is possibly because the macropores in a foam-like microstructure of CID-NO<sub>2</sub>-1000 provide better diffusion of ions throughout the carbon electrode. Among the carbon samples, ZnNipdpe-1000 exhibits the highest capacitance at all tested sweep rates. The highest specific capacitance is 130 F g<sup>-1</sup> at 2 mV s<sup>-1</sup>, which is about 75% and 60% higher than CID-H-1000 and CID-NO<sub>2</sub>-1000, respectively. Note that although ZnNipdpe-1000 has similar BET surface area and pore volume as of CID-NO<sub>2</sub>-1000, but the sample has more uniform pore size distribution. Cooperative effect of the designed microstructure in the well-ordered pore structures of carbon provides a significant improvement of the specific capacitance.

## Conclusions

We focused on the thermal chemical process of organic ligands in PCPs to prepare porous carbon with a variety of morphologies by carbonization. Among several organic groups, the nitro group is crucial for the preparation of porous carbon with a foam-like microstructure due to the fast kinetics of gas evolution during

carbonization. The foam-like microstructure improved the specific capacitance of porous carbon, which is useful for the

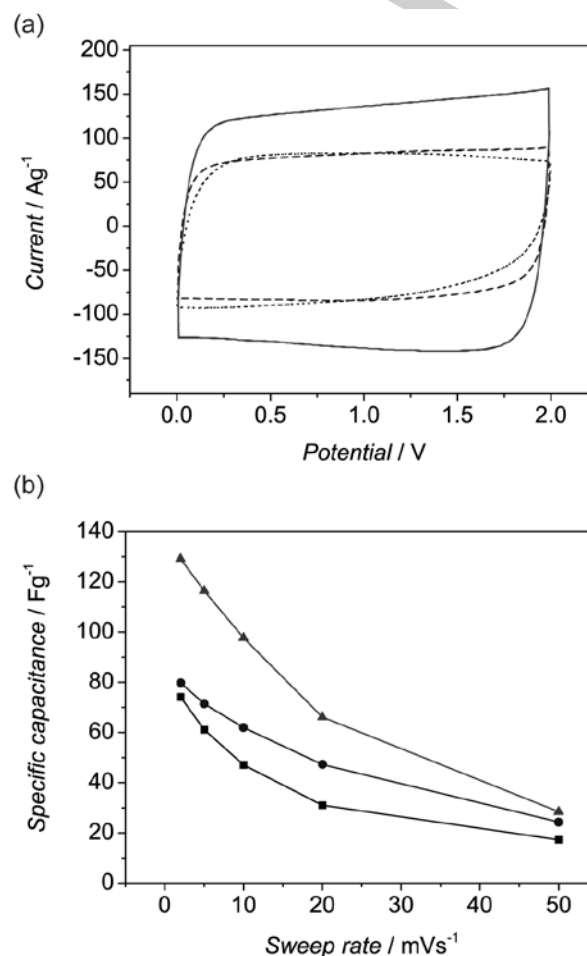


**Figure 7.** (a) Cyclic voltammograms at 2 mV s<sup>-1</sup> for CID-H-1000 (dot), CID-NO<sub>2</sub>-1000 (dash) and ZnNipdpe-1000 (solid line). (b) Specific capacitances of CID-H-1000 (squares), CID-NO<sub>2</sub>-1000 (circles) and ZnNipdpe-1000 (triangles) at different sweep rates.

design of carbon-based materials for EDLC. Although ligand-directed design of porous carbon by use of PCPs has rarely been studied, the strategy is feasible to control microstructures and other properties of carbon materials by tuning the chemical process of organic ligands in PCP/MOFs during carbonization.

## Experimental Section

**Syntheses of porous carbons.** All PCPs were synthesized in a large scale according to previously reported procedure.<sup>[8a, 9, 15]</sup> Carbonization of PCPs was carried out in a tube furnace (30-mm tube diameter) under a flow of N<sub>2</sub> (200 mL min<sup>-1</sup>). Typically, 300 mg of guest-free PCP powder was placed on a ceramic boat (16 mm × 12 mm × 80 mm). All CID-R were heated up to the targeted temperature with a heating rate 10 °C

min<sup>-1</sup> and held for 15 minutes before cooling. [Zn(NO<sub>2</sub>-ip)(bpe)]<sub>n</sub> was heated at 1000 °C for 2 hours under the same furnace setting as CID-R.

**Characterization.** Powder X-ray diffraction (PXRD) data were collected on a Rigaku RINT 2200 Ultima diffractometer with Cu K $\alpha$  radiation. Thermogravimetric analysis combined with differential thermal analysis (TG-DTA) data was measured up to 1200 °C under flowing N<sub>2</sub> with 10 °C min<sup>-1</sup> ramp rate on a Rigaku TG8120. Thermogravimetric analysis combined with mass spectrometry (TG-MS) was measured up to 900 °C with 10 °C min<sup>-1</sup> ramp rate on a Rigaku TG8120. Thermogravimetric analysis combined with mass spectrometry (TG-MS) was measured up to 900 °C with 10 °C min<sup>-1</sup> ramp rate under a flow of Helium on a Rigaku Thermo plus EVO II equipped with ThermoMass Photo/S. N<sub>2</sub> adsorption isotherms were measured at -196 °C by BELSORP-mini. All samples were activated by heating at 180 °C under reduced pressure (< 10<sup>-2</sup> Pa) overnight before gas adsorption measurements. Raman spectra were collected at room temperature by using a LabRAM HR800 (Horiba Jobin Yvon) with a semiconductor laser at 488 nm. Scanning electron microscope data was collected by using a Hitachi S-30000N SEM system operated at an accelerating voltage of 20 kV. Transmission electron microscopic (TEM) observations were performed by using JEOL JEM1400D. TEM specimens were prepared by dropping methanol solutions containing the samples on Cu grids. Electrochemical measurements were carried out on VersaSTAT-4 system at room temperature using a standard two-electrode configuration.

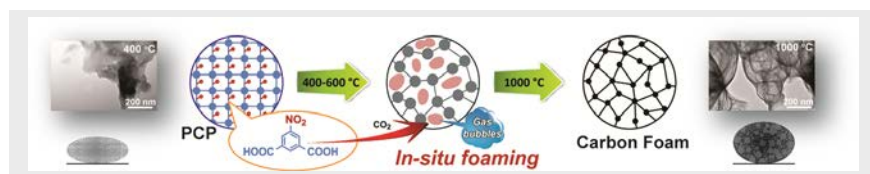
## Acknowledgements

This work was supported by a Grant-in-Aid for Scientific Research on the Innovative Areas: "Fusion Materials", Grant-in-Aid for Young Scientists (A), Grant-in-Aid for Challenging Exploratory Research from the Ministry of Education, Culture, Sports, Science and Technology (MEXT), Japan and the PRESTO program of the Japan Science and Technology Agency (JST), and World Premier International Research Center Initiative on Institute for Integrated Cell-Material Sciences (WPI-iCeMS) from MEXT, Japan.

- [1] a) R. Ryoo, S. H. Joo, M. Kruk, M. Jaroniec, *Adv. Mater.* **2001**, *13*, 677-681; b) J. Lee, J. Kim, T. Hyeon, *Adv. Mater.* **2006**, *18*, 2073-2094; c) C. Liang, Z. Li, S. Dai, *Angew. Chem. Int. Ed.* **2008**, *47*, 3696-3717; d) N. Linares, A. M. Silvestre-Albero, E. Serrano, J. Silvestre-Albero, J. Garcia-Martinez, *Chem. Soc. Rev.* **2014**, *43*, 7681-7717; e) S. Rondeau-Gagné, J.-F. Morin, *Chem. Soc. Rev.* **2014**, *43*, 85-98.
- [2] a) A. H. Lu, F. Schüth, *Adv. Mater.* **2006**, *18*, 1793-1805; b) T. Morishita, T. Tsumura, M. Toyoda, J. Przepiórski, A. W. Morawski, H. Konno, M. Inagaki, *Carbon* **2010**, *48*, 2690-2707; c) H. Nishihara, T. Kyotani, *Adv. Mater.* **2012**, *24*, 4473-4498.
- [3] a) B. Liu, H. Shioyama, T. Akita, Q. Xu, *J. Am. Chem. Soc.* **2008**, *130*, 5390-5391; b) S. J. Yang, T. Kim, J. H. Im, Y. S. Kim, K. Lee, H. Jung, C. R. Park, *Chem. Mater.* **2012**, *24*, 464-470; c) K. Xi, S. Cao, X. Peng, C. Ducati, R. Vasant Kumar, A. K. Cheetham, *Chem. Commun.* **2013**, *49*, 2192-2194; d) W. Chaikittisilp, K. Ariga, Y. Yamauchi, *J. Mater. Chem. A* **2013**, *1*, 14-19; e) J.-K. Sun, Q. Xu, *Energy Environ. Sci.* **2014**, *7*, 2071; f) K. M. Choi, H. M. Jeong, J. H. Park, Y.-B. Zhang, J. K. Kang, O. M. Yaghi, *ACS Nano* **2014**, *8*, 7451-7457; g) M. C. So, G. P. Wiederrecht, J. E. Mondloch, J. T. Hupp, O. K. Farha, *Chem. Commun.* **2015**, *51*, 3501-3510; h) L. Wang, X. Feng, L. Ren, Q. Piao, J. Zhong, Y. Wang, H. Li, Y. Chen, B. Wang, *J. Am. Chem. Soc.* **2015**, *137*, 4920-4923.
- [4] a) E. Proietti, F. Jaouen, M. Lefèvre, N. Larouche, J. Tian, J. Herranz, J.-P. Dodelet, *Nat Commun* **2011**, *2*, 416; b) M. Hu, J. Reboul, S. Furukawa, N. L. Torad, Q. Ji, P. Srinivasu, K. Ariga, S. Kitagawa, Y. Yamauchi, *J. Am. Chem. Soc.* **2012**, *134*, 2864-2867; c) A. Aijaz, N. Fujiwara, Q. Xu, *J. Am. Chem. Soc.* **2014**, *136*, 7490-7493; d) F. Zheng, Y. Yang, Q. Chen, *Nat. Commun.* **2014**, *5*; e) H. J. Lee, S. Choi, M. Oh, *Chem. Commun.* **2014**, *50*, 4492-4495; f) H. J. Lee, W. Cho, E. Lim, M. Oh, *Chem. Commun.* **2014**, *50*, 5476-5479; g) W. Chaikittisilp, N. L. Torad, C. Li, M. Imura, N. Suzuki, S. Ishihara, K. Ariga, Y. Yamauchi, *Chem. Eur. J.* **2014**, *20*, 4217-4221; h) S. Pandiaraj, H. B. Aiyappa, R. Banerjee, S. Kurungot, *Chem. Commun.* **2014**, *50*, 3363-3366.
- [5] a) N. C. Gallego, J. W. Klett, *Carbon* **2003**, *41*, 1461-1466; b) C. Chen, E. B. Kennel, A. H. Stiller, P. G. Stansberry, J. W. Zondlo, *Carbon* **2006**, *44*, 1535-1543; c) A. V. Rode, S. T. Hyde, E. G. Gamaly, R. G. Elliman, D. R. McKenzie, S. Bulcock, *Appl. Phys. A* **1999**, *69*, S755-S758.
- [6] a) A. V. Rode, E. G. Gamaly, B. Luther-Davies, *Appl. Phys. A* **2000**, *70*, 135-144; b) A. Zani, D. Dellasega, V. Russo, M. Passoni, *Carbon* **2013**, *56*, 358-365.
- [7] a) J. Lee, K. Sohn, T. Hyeon, *J. Am. Chem. Soc.* **2001**, *123*, 5146-5147; b) M. Inagaki, T. Morishita, A. Kuno, T. Kito, M. Hirano, T. Suwa, K. Kusakawa, *Carbon* **2004**, *42*, 497-502; c) X.-h. Yang, P. He, Y.-y. Xia, *Electrochem. Commun.* **2009**, *11*, 1127-1130; d) S. Chen, G. He, H. Hu, S. Jin, Y. Zhou, Y. He, S. He, F. Zhao, H. Hou, *Energy Environ. Sci.* **2013**, *6*, 2435-2439.
- [8] a) S. Horike, D. Tanaka, K. Nakagawa, S. Kitagawa, *Chem. Commun.* **2007**, 3395-3397; b) C. Ma, C. Chen, Q. Liu, D. Liao, L. Li, L. Sun, *New J. Chem.* **2003**, *27*, 890-894; c) J. Tao, X.-M. Chen, R.-B. Huang, L.-S. Zheng, *J. Solid State Chem.* **2003**, *170*, 130-134; d) Y.-H. Wen, J.-K. Cheng, Y.-L. Feng, J. Zhang, Z.-J. Li, Y.-G. Yao, *Inorg. Chim. Acta* **2005**, *358*, 3347-3354; e) G. Tian, G. Zhu, Q. Fang, X. Guo, M. Xue, J. Sun, S. Qiu, *J. Mol. Struct.* **2006**, *787*, 45-49.
- [9] T. Fukushima, S. Horike, Y. Inubushi, K. Nakagawa, Y. Kubota, M. Takata, S. Kitagawa, *Angew. Chem. Int. Ed.* **2010**, *49*, 4820-4824.
- [10] T. B. Brill, K. J. James, *Chem. Rev.* **1993**, *93*, 2667-2692.
- [11] a) J. Hu, H. Wang, Q. Gao, H. Guo, *Carbon* **2010**, *48*, 3599-3606; b) W. Chaikittisilp, M. Hu, H. Wang, H.-S. Huang, T. Fujita, K. C. W. Wu, L.-C. Chen, Y. Yamauchi, K. Ariga, *Chem. Commun.* **2012**, *48*, 7259-7261; c) T. Palaniselvam, B. P. Biswal, R. Banerjee, S. Kurungot, *Chem. Eur. J.* **2013**, *19*, 9335-9342.
- [12] T. Jawhari, A. Roid, J. Casado, *Carbon* **1995**, *33*, 1561-1565.
- [13] K. S. W. Sing, *Pure Appl. Chem.* **1985**, *57*, 603-619.
- [14] L. J. M. Jacobs, M. F. Kemmere, J. T. F. Keurentjes, *Green Chem.* **2008**, *10*, 731-738.
- [15] S. Horike, K. Kishida, Y. Watanabe, Y. Inubushi, D. Umeyama, M. Sugimoto, T. Fukushima, M. Inukai, S. Kitagawa, *J. Am. Chem. Soc.* **2012**, *134*, 9852-9855.

## Entry for the Table of Contents (Layout 2)

## FULL PAPER



Kanokwan Kongpatpanich, Satoshi Horike,\* Yu-ichi Fujiwara, Naoki Ogiwara, Hiroto Nishihara, Susumu Kitagawa\*

**Page No. – Page No.**

**Formation of Foam-like Microstructural Carbon by Carbonization of Porous Coordination Polymers via Ligand-assisted Foaming Process**